

Subsolidus binary phase diagram of $(n\text{-C}_n\text{H}_{2n+1}\text{NH}_3)_2\text{ZnCl}_4$ ($n = 14, 16, 18$)

Kezhong Wu · Jianjun Zhang

Received: 30 August 2009 / Accepted: 13 April 2010 / Published online: 6 May 2010
© Akadémiai Kiadó, Budapest, Hungary 2010

Abstract The thermotropic phase solid–solid transitions compound $(n\text{-C}_n\text{H}_{2n+1}\text{NH}_3)_2\text{ZnCl}_4$ ($n = 14, 16, 18$) were studied, and a series of their mixtures were prepared. These laminar materials contain bilayers sandwiched between metal halide layers. The low temperature crystal structures of the pure salts are characteristic of the piling of sandwiches in which a two-dimensional macro-anion ZnCl_4^{2-} is sandwiched between two alkylammonium layers. These layers become conformationally disordered in the high temperature phases. The subsolidus binary phase diagrams of $(n\text{-C}_{14}\text{H}_{29}\text{NH}_3)_2\text{ZnCl}_4$ – $(n\text{-C}_{18}\text{H}_{37}\text{NH}_3)_2\text{ZnCl}_4$ and $(n\text{-C}_{16}\text{H}_{33}\text{NH}_3)_2\text{ZnCl}_4$ – $(n\text{-C}_{18}\text{H}_{37}\text{NH}_3)_2\text{ZnCl}_4$ were established by differential thermal analysis and X-ray diffraction. In each phase diagram, an intermediate compound and two eutectoid invariants were observed. There are three noticeable solid solution ranges (α , β , γ) at the left boundary, right boundary, and middle of the phase diagram.

Keywords Tetradecylammonium tetrachlorozincate · Hexadecylammonium tetrachlorozincate · Octadecylammonium tetrachlorozincate · Phase diagram · Differential thermal analysis

Introduction

The investigation of perovskite type compounds with the general formula $(n\text{-C}_n\text{H}_{2n+1}\text{NH}_3)_2\text{MCl}_4$ ($\text{M}=\text{Cu}, \text{Mn}, \text{Cd}$,

Zn, Co , etc.) (short notation; C_nM) has greatly contributed to our understanding of phase transitions in layer structures [1, 2]. All the compounds show solid–solid order–disorder phase transitions below 373 K. Layered organic–inorganic hybrid compounds have been widely studied, since they can, in principle, combine properties of the inorganic and organic parts within a single system [3]. The advances in synthesis along with the ease of controlling various structural parameters (metal, halogen, and number of carbon atoms in the alkylammonium ion) have made them ideal objects for studies by spectroscopy, calorimetry, diffraction, and a variety of other techniques [4]. In the case of C_nZn , parallel sheets of corner-sharing ZnCl_4^{2-} tetrahedra are held together by the n -alkylammonium groups. The $-\text{NH}_3^+$ groups of the chains occupy the cavities of the ZnCl_4^{2-} layers and are bonded by hydrogen bonds to the chlorine atoms [5]. Applications of such materials include the development of functional magnetic, electronic, and optoelectronic materials [6]. The physical properties and structures of C_nM [7–9] have been previously researched. The binary subsolidus phase diagrams for C_{10}Zn – C_{12}Zn [10], C_{10}Zn – C_{16}Zn [11, 12], C_{12}Zn – C_{16}Zn [11, 12], C_{12}Zn – C_{18}Zn [13], C_{14}Zn – C_{16}Zn [14], C_{10}Mn – C_{14}Mn [15], and C_{12}Mn – C_{16}Mn [16, 17] have been reported. Among them, C_{10}Zn – C_{16}Zn [12] and C_{12}Mn – C_{16}Mn [16] show absolute immiscibility. As we know, the binary phase diagrams of C_{14}Zn – C_{18}Zn and C_{16}Zn – C_{18}Zn have not been studied, in this study we synthesized three types of materials of $[\text{NR}_4]_2\text{ZnCl}_4$ in bis (n -alkylammonium) tetrachlorozincate (II) with the general formula $(n\text{-C}_{14}\text{H}_{29}\text{NH}_3)_2\text{ZnCl}_4$ (C_{14}Zn), $(n\text{-C}_{16}\text{H}_{33}\text{NH}_3)_2\text{ZnCl}_4$ (C_{16}Zn), and $(n\text{-C}_{18}\text{H}_{37}\text{NH}_3)_2\text{ZnCl}_4$ (C_{18}Zn). The subsolidus phase diagrams of C_{14}Zn – C_{18}Zn and C_{16}Zn – C_{18}Zn were established by differential thermal analysis (DTA) and X-ray diffraction (XRD).

K. Wu (✉) · J. Zhang

Department of Chemistry and Material Science, Key Laboratory of Inorganic Nano-materials of Hebei Province, Hebei Normal University, 113 YuHua Rd., Shijiazhuang 050016, China
e-mail: wukzh688@163.com

Experimental procedure

ZnCl_2 , concentrated HCl, and absolute ethanol used were analytical grade. Tetradecylamine was purchased from Beijing Chemical Plant. Hexadecylamine (A.P.) was purchased from ACROS ORGANICS (Germany) and Octadecylamine (C.P.) from Beijing Xudong Reagent Plant.

For the synthesis of C_nZn , the hot absolute ethanol solutions of ZnCl_2 , concentrated HCl, and the corresponding alkylamine were mixed in a 1:2:2 M ratio. The solutions were concentrated by boiling for 30 min and then cooled to room temperature. After filtration, the products were recrystallized twice from absolute ethanol. Finally, they were placed in a vacuum desiccator for 8 h at about 353 K. C_{14}Zn , C_{16}Zn , and C_{18}Zn were analyzed with an MT-3 CHN elemental analyzer (Japan). Elemental analyses calc.(%) for C_{14}Zn : C 52.82, H 10.06, N 4.40, Cl 22.36; Found: C 53.00, H 10.25, N 4.34, Cl 22.19. Anal. Calcd. For C_{16}Zn : C 55.53, H 10.49, N 4.05, Cl 20.49; Found: C 55.65, H 10.77, N 4.19, Cl 20.52. Anal. Calcd. For C_{18}Zn : C 57.79, H 10.78, N 3.75, Cl 19.01; Found: C 57.07, H 10.45, N 3.72, Cl 20.02. The C_nZn were weighed exactly in the desired proportions to prepare the mixed samples of $\text{C}_{14}\text{Zn}-\text{C}_{18}\text{Zn}$ and $\text{C}_{16}\text{Zn}-\text{C}_{18}\text{Zn}$. The two components were dissolved in absolute ethanol and then the solvent was evaporated. The samples were dried in a vacuum desiccators for 8 h at a temperature of about 353 K. The concentrations of all materials in the binary system were expressed as $W_{\text{C}_{18}\text{Zn}}\%$.

The DTA curve was measured on a CDR-4P differential scanning calorimeter (Shanghai Scale Instrument Plant) at a scanning rate of 5 K/min in a static atmosphere. Samples of about 4.5 mg were sealed in aluminum crucibles. XRD patterns on compacted samples of the powders were taken with a D/MAX-RA X-ray diffractometer (made in Japan) using Cu K_α radiation (Ni filter) at a scanning rate of 2° min^{-1} . The voltage and electric current were 40 kV and 100 mA, respectively.

Results and discussion

Thermal analysis

The $\text{C}_{14}\text{Zn}-\text{C}_{18}\text{Zn}$ binary systems were examined in the entire composition range and in a temperature range of 340 to 380 K. Figure 1 shows some typical DTA curves with different $W_{\text{C}_{18}\text{Zn}}\%$. The results of the DTA experiments obtained using the “Shape factors method” [18] are listed in Table 1. All the $\text{C}_{14}\text{Zn}-\text{C}_{18}\text{Zn}$ binary systems show solid–solid phase transitions in the temperature range of 340 to 380 K. The data in Table 1 show that the value of the transition temperature decreases with increasing

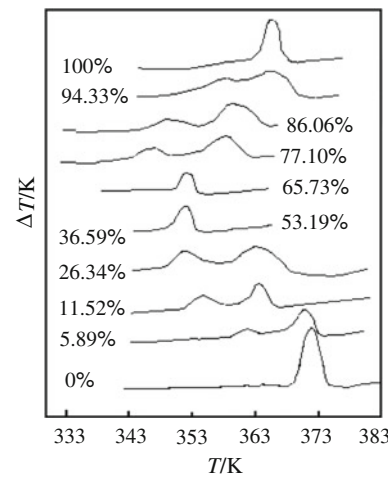


Fig. 1 DTA curves of $\text{C}_{14}\text{Zn}-\text{C}_{18}\text{Zn}$ with different $W_{\text{C}_{18}\text{Zn}}\%$

Table 1 Solid–solid transition temperatures for the $\text{C}_{14}\text{Zn}-\text{C}_{18}\text{Zn}$ binary systems with different $W_{\text{C}_{18}\text{Zn}}\%$

$W_{\text{C}_{18}\text{Zn}}\%$	T_{e1}/K	T_{e2}/K	T_{s1}/K	T_{s2}/K
0(C_{14}Zn)			369	
2.31			363	368
5.89			359	367
11.52			353	365
16.00	349			364
20.88	348			361
26.34	348			359
31.33	349			357
33.28	348			356
36.59	349			354
40.76	349			350
44.59	349			351
49.81	349			353
53.19			351	354
57.19			351	355
61.14	343			354
65.73	342			353
69.34	342			349
74.49	342			352
77.10	343			355
80.58	342			356
86.06			346	358
89.85			349	359
94.33			353	361
100(C_{18}Zn)			362	

T_e eutectoid invariant, T_s solid–solid transition temperature

$W_{\text{C}_{18}\text{Zn}}\%$ in the range from 0 to 42.62%. Then, the phase transition temperature first rises with $W_{\text{C}_{18}\text{Zn}}\%$ from 42.62 to 57.19%. The first eutectoid temperature (about 349 K)

Table 2 d values for C_{14}Zn , C_{18}Zn , and their binary systems with different $W_{\text{C}_{18}\text{Zn}}\%$ at room temperature

C_{14}Zn	5.89%	11.52%	26.34%	36.59%	53.19%	65.73%	77.10%	86.06%	94.53%	C_{18}Zn
7.734	7.734	7.056	7.050	7.053	7.517	7.061	7.085	7.084	7.094	7.054
5.847	6.028	6.530	6.409	6.500	6.422	6.034	6.058	6.024	6.423	6.528
5.188	5.010	5.912	6.021	6.001	5.946	5.890	5.890	5.328	5.372	5.901
4.927	4.961	4.965	5.859	5.882	5.675	5.625	5.404	5.253	5.117	5.456
4.799	4.321	4.557	5.498	5.372	5.556	5.455	5.155	4.741	4.755	4.961
4.252	4.127	4.136	5.050	5.033	5.098	5.004	5.044	4.237	4.186	4.128
4.112	3.645	3.665	4.960	4.912	4.912	4.912	4.860	4.161	3.948	3.644
3.636	3.425	3.432	4.739	4.734	4.873	4.739	4.734	4.107	3.689	3.422
3.371	3.061	3.061	4.483	4.492	4.491	4.488	4.498	3.953	3.108	3.061
2.947	2.985	2.987	4.179	4.179	4.215	4.186	4.117	3.623	3.051	2.937
		2.536	3.686	3.683	3.987	3.892	3.975	3.430	2.753	2.537
		2.918	3.434	3.434	3.432	3.432	3.698	3.380	2.648	2.087
			3.106	3.108	3.108	3.116	3.290	2.956		
			3.044	3.041	2.932	2.934	2.842	2.782		
			2.915	2.932		2.668	3.580			
			2.635	2.661		2.572	2.684			
						2.109	2.188			

appears in the $W_{\text{C}_{18}\text{Zn}}\%$ range of 16.00 to 49.81%. The phase transition temperature decreases again with $W_{\text{C}_{18}\text{Zn}}\%$ from 57.19 to 71.43% and then rises with the increasing $W_{\text{C}_{18}\text{Zn}}\%$. The second eutectoid temperature at about 342 K was found in the $W_{\text{C}_{18}\text{Zn}}\%$ range of 61.14 to 80.58%. Table 1 reveals that the first eutectoid temperature is not close to that pure C_{14}Zn $W_{\text{C}_{18}\text{Zn}}\% = 0$, nor does the second eutectoid temperature end near that of pure C_{18}Zn $W_{\text{C}_{18}\text{Zn}}\% = 100\%$. The range of the first eutectoid temperature does not end close to the beginning of the second eutectoid temperature. It is clear that the phase transition temperatures of the binary system $\text{C}_{14}\text{Zn}-\text{C}_{18}\text{Zn}$ in solid-solid phase transitions show a strong dependence on $W_{\text{C}_{18}\text{Zn}}\%$. The reason is that there are not only intermediates of the form $(n\text{-C}_{14}\text{H}_{29}\text{NH}_3)(n\text{-C}_{18}\text{H}_{37}\text{NH}_3)\text{ZnCl}_4$ (short notation: $\text{C}_{14}\text{C}_{18}\text{Zn}$) but also three solid solution ranges existing at the left boundary, right boundary and middle of the phase diagram of $\text{C}_{14}\text{Zn}-\text{C}_{18}\text{Zn}$.

X-ray diffraction

Table 2 summarizes the d values of strong peaks with bigger relative intensity at room temperature for pure C_{14}Zn , C_{18}Zn , and their binary systems. It is found that d values of sample from 5.89 to 11.52% are similar to that of pure C_{14}Zn , indicating a single-phase region. In this concentration range from pure C_{14}Zn $W_{\text{C}_{18}\text{Zn}}\% = 0 - 16.00\%$, $\text{C}_{14}\text{C}_{18}\text{Zn}$ dissolves in C_{14}Zn to form a solid solution α . Similarly, samples with $W_{\text{C}_{18}\text{Zn}}\%$ from 80.58% to pure C_{18}Zn $W_{\text{C}_{18}\text{Zn}}\% = 100\%$ have homologous patterns, revealing that the $\text{C}_{14}\text{C}_{18}\text{Zn}$ dissolves in C_{18}Zn to

form a solid solution β . In the same way, $\text{C}_{14}\text{Zn}-\text{C}_{18}\text{Zn}$ samples with $W_{\text{C}_{18}\text{Zn}}\%$ from 49.81 to 61.14% have similar diffraction patterns, showing that C_{14}Zn or C_{18}Zn dissolved in $\text{C}_{14}\text{C}_{18}\text{Zn}$ forms a single-phase γ . $\text{C}_{14}\text{Zn}-\text{C}_{18}\text{Zn}$ samples with $W_{\text{C}_{18}\text{Zn}}\%$ from 16.00 to 49.81% are in the two-phase region, and their patterns are an overlap of α and γ . The XRD patterns of $\text{C}_{14}\text{Zn}-\text{C}_{18}\text{Zn}$ samples with the $W_{\text{C}_{18}\text{Zn}}\%$ range of 61.14 to 80.58% are an overlap of β and γ and thus in the two-phase region.

Establishment of phase diagram

The subsolidus binary phase diagram of $\text{C}_{14}\text{Zn}-\text{C}_{18}\text{Zn}$ (Fig. 2) was constructed according to the temperature-composition relations from the DTA and XRD experiments. The subsolidus curve in Fig. 2 indicates the maximum temperature of 354 K at an equimass ratio of $(n\text{-C}_{14}\text{H}_{29}\text{NH}_3)_2\text{ZnCl}_4$ to $(n\text{-C}_{18}\text{H}_{37}\text{NH}_3)_2\text{ZnCl}_4$ (40.36% C_{14}Zn , 59.64% C_{18}Zn). This composition corresponds to the stoichiometry of an intermediate compound $(n\text{-C}_{14}\text{H}_{29}\text{NH}_3)(n\text{-C}_{18}\text{H}_{37}\text{NH}_3)\text{ZnCl}_4$ which is formed between two eutectoid invariants [19–21]. The low temperature perovskite-layer structure of C_{14}Zn , C_{18}Zn , and their binary system are organized by neutralizing ZnCl_4^{2-} with alkylammonium ions. Alkylammonium chains lie parallel to each other and are slightly tilted with respect to the normal of the inorganic layers. The adjacent alkyl chains interact with each other by van der Waals interactions and are hydrogen bonded to ZnCl_4^{2-} . When the temperature is increased to 349 K, the first eutectoid invariant occurs with $W_{\text{C}_{18}\text{Zn}}\%$ from 16.00 to 49.81%. C_{14}Zn and $\text{C}_{14}\text{C}_{18}\text{Zn}$

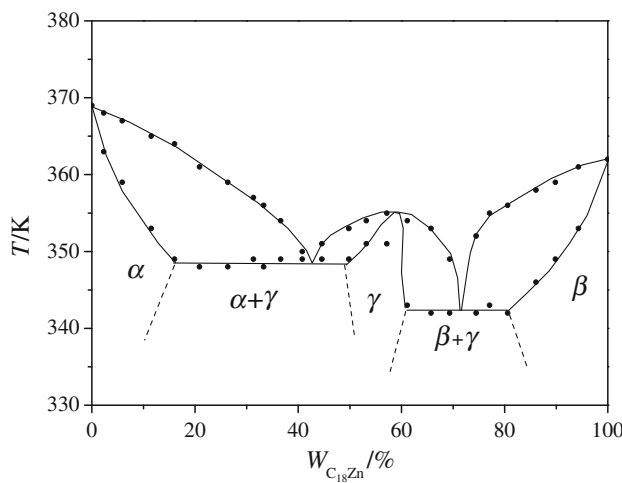


Fig. 2 Phase diagram of the $C_{14}Zn-C_{18}Zn$ system

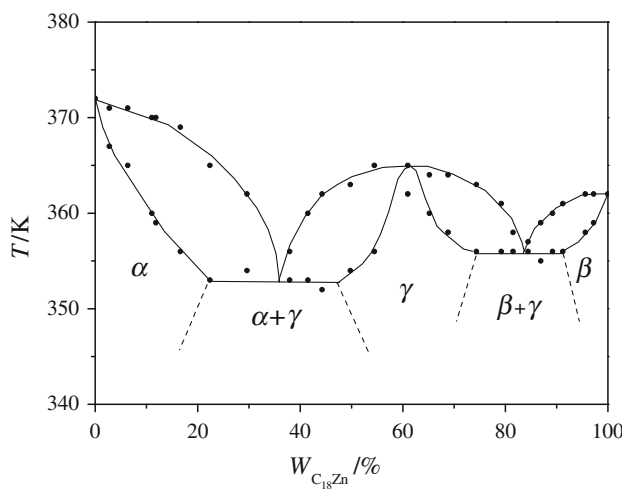


Fig. 3 Phase diagram of the $C_{16}Zn-C_{18}Zn$ system

undergo a reversible solid–solid phase transformation. In this situation, the chains possess a large degree of motional freedom and a disordered phase appears. At the same time, the hydrogen bonds are weakened and even destroyed. The second eutectoid invariant appears with $W_{C_{18}Zn} \%$ from 61.14 to 80.58% at 342 K. Similarly, $C_{18}Zn$ and $C_{14}C_{18}Zn$ undergo a reversible solid–solid phase transformation.

The subsolidus binary phase diagram of $C_{16}Zn-C_{18}Zn$ was obtained in the same way (see Fig. 3). The first eutectoid temperature 353 K appears in the $W_{C_{18}Zn} \%$ range from 22.39 to 47.51%. The second eutectoid temperature at about 356 K was found in the $W_{C_{18}Zn} \%$ range from 74.37 to 91.20%. Simultaneously, an intermediate compound ($n\text{-}C_{16}H_{33}NH_3$) $(n\text{-}C_{18}H_{37}NH_3)ZnCl_4$ ($C_{16}C_{18}Zn$) and two eutectoid invariants were observed. There are three noticeable solid solution ranges (α , β , δ) at the left boundary, right boundary, and middle of the phase diagram. The phase diagrams of $C_{14}Zn-C_{18}Zn$ and $C_{16}Zn-C_{18}Zn$

obtained in this study are similar to that of $C_{14}Zn-C_{16}Zn$ which has been reported in our previous work [14]. For the intermediate compound of these three binary systems, the mass ratio between the two n -alkylammonium groups is 2:3. However, the phase diagrams of $C_{14}Zn-C_{18}Zn$ and $C_{16}Zn-C_{18}Zn$ obtained in this study are different from those of the other homologous systems of $C_{10}Zn-C_{16}Zn$ [12] and $C_{12}Mn-C_{16}Mn$ [16]. Partial miscibility was observed for the binary systems in this study, while the latter two binary systems show absolute immiscibility. This can be attributed to the difference in the molecular structure and size of the two compounds in the binary system, i.e., the degree of the miscibility can be improved by the reducing the differences in molecular structure and size.

Conclusions

The subsolidus binary phase diagrams of $C_{14}Zn-C_{18}Zn$ and $C_{16}Zn-C_{18}Zn$ mixtures were established by DTA and XRD in the temperature interval 340–370 K. The two eutectoid occur in the $C_{14}Zn-C_{18}Zn$ system: e_1 at 349 ± 1 K for $W_{C_{18}Zn} \% = 42.78\%$ and e_2 at $342 K \pm 1$ K for $W_{C_{18}Zn} \% = 71.43\%$, other two eutectoid occur in the $C_{16}Zn-C_{18}Zn$ system: e_1 at 353 ± 1 K for $W_{C_{18}Zn} \% = 35.76\%$ and e_2 at 356 ± 1 K for $W_{C_{18}Zn} \% = 83.43\%$. Their phase diagrams are very similar, belonging to a partially miscible system. Intermediate compounds of $(n\text{-}C_{14}H_{29}NH_3)(n\text{-}C_{18}H_{37}NH_3)ZnCl_4$ and $(n\text{-}C_{16}H_{33}NH_3)(n\text{-}C_{18}H_{37}NH_3)ZnCl_4$ ($C_{16}C_{18}Zn$) were observed in $C_{14}Zn-C_{18}Zn$ and $C_{16}Zn-C_{18}Zn$ system, respectively. There are three noticeable solid solution ranges, at the left boundary, right boundary, and middle of the phase diagram. It is revealed that the crystal structure and the size of the molecule are the essential factors that affect the miscibility of the binary systems.

Acknowledgements This project was financially supported by National Natural Science Foundation of China (No. 20773034), Natural Science Foundation of Hebei Province (No. E2009000307), Education Department Scientific Research Fund from Hebei Province (No. 2008469), and Science Foundation of Hebei Normal University (L2006B16, L2008Z07).

References

1. Avitabile G, Ciajolo MR, Napolitano R, Tuzi A. Comparative studies of layer structure: the crystal structures of bis(*mono-n*-dodecylammonium) tetrabromozincate and bis(*mono-n*-tridecylammonium) tetrabromozincate. *Gazz Chim Ital.* 1983;113:475–9.
2. Anna M-M, Joanna H. Thermal behavior of $[Ca(H_2O)_4](ClO_4)_2$ and $[Ca(NH_3)_6](ClO_4)_2$. *J Therm Anal Calorim.* 2008;91:529–34.
3. Venkataraman NV, Barman S, Vasudevan S, Seshadri R. Structural analysis of alkyl chain conformation in the layered organic–inorganic hybrid $[(C_{n}H_{2n+1})NH_3]_2PbI_4$ ($n = 12, 16, 18$) by spectroscopy. *Chem Phys Lett.* 2002;358:139–43.

4. Schenk KJ, Chapuis G. Thermotropic phase transitions in bis (*n*-tetradecylammonium) tetrachlorocadmate(II) and some homologous compounds. *J Phys Chem.* 1988;92:7141–7.
5. Ciajolo MR, Corradini P, Pavone V. Bis(*n*-dodecylammonium)Tetrachlorozincate. *Acta Cryst.* 1977;33:553–5.
6. Gósnowska M, Ciunika Z, Batora G, Jakubasa R, Baranb J. Structure and phase transitions in tetramethylammonium tetrabromoindate(III) and tetraethylammonium tetrabromoindate(III) crystals. *J Mol Struct.* 2000;555:243–55.
7. Lv XC, Tan ZC, Gao XH, Shi Q, Sun LX. Molar heat capacity and thermodynamic properties of crystalline $[\text{Nd}(\text{Glu})(\text{H}_2\text{O})_5(\text{Im})_3](\text{ClO}_4)_6\text{H}_2\text{O}$. *J Therm Anal Calorim.* 2009;95:387–92.
8. Wu KZ, Li JL, Zhang JJ, Liu XD. Nonisothermal kinetics of the solid-solid phase transitions in the perovskite type layer compounds $(\text{C}_n\text{H}_{2n+1}\text{NH}_3)_2\text{ZnCl}_4$. *Chin J Chem.* 2008;26:216–9.
9. Busico V, Tartaglione T, Vacatello M. The thermal behavior of mixed long chain alkylammonium tetracholomanganates(II). *Thermochim Acta.* 1983;62:77–86.
10. Wu KZ, Zuo P, Liu XD, Li YJ. Subsolidus binary phase diagram of $\text{C}_{10}\text{Zn}/\text{C}_{12}\text{Zn}$. *Thermochim Acta.* 2003;397:49–53.
11. Wu KZ, Zhang CX, Li YJ, Liu XD. Subsolidus binary phase diagrams of $\text{C}_{10}\text{ZnCl}-\text{C}_{16}\text{ZnCl}$ and $\text{C}_{12}\text{ZnCl}-\text{C}_{16}\text{ZnCl}$. *J Chin Chem Soc.* 2005;52:45–50.
12. Ruan DS, Li WP, He LF, Hu QH. Phase diagrams of binary systems of alkylammonium tetrachlorometallates(II). *J Therm Anal.* 1995;45:235–42.
13. Wu KZ, Wang XD, Liu XD. Phase diagram of binary system $\text{C}_{12}\text{Zn}-\text{C}_{18}\text{Zn}$. *J Univ Sci Technol Beijing.* 2003;10:75–7.
14. Kang YZ, Hao ZF, Zhang CX, Wu KZ, Liu XD. Phase diagram of binary system $(\text{C}_{14}\text{H}_{29}\text{NH}_3)_2\text{ZnCl}_4-(\text{C}_{16}\text{H}_{33}\text{NH}_3)_2\text{ZnCl}_4$. *Chem Res Appl.* 2004;16(6):761–4.
15. Wu KZ, Zhang JJ. Subsolidus phase diagram of binary system in the perovskite type layer compounds $(n\text{-C}_n\text{H}_{2n+1}\text{NH}_3)_2\text{MnCl}_4$. *J Therm Anal Calorim.* 2009;95:589–93.
16. Salerno V, Grieco A, Vacatello M. Ordered and disorder phase in mixed dodecylammonium and hexadecylammonium retrachloromanganate (II). *J Phys Chem.* 1976;80:2444.
17. Wu KZ, Cui WZ, Zhang JJ. Subsolidus binary phase diagram of $\text{C}_{12}\text{Mn}-\text{C}_{16}\text{Mn}$ in thermotropic phase transitions materials. *Thermochim Acta.* 2007;463:15–7.
18. Courchinoux R, Chanh NB, Haget Y. Use of the “shape factors” as an empirical method to determine the actual characteristic temperatures of binary phase diagrams by differential scanning calorimetry. *Thermochim Acta.* 1988;128:45–53.
19. Turkin AI, Drebushchak VA. Solid solution the $\text{MgO}-\text{Al}_2\text{O}_3-\text{Cr}_2\text{O}_3$ system. *J Therm Anal Calorim.* 2009;95:81–6.
20. Nakamura GHG, Baldochi SL, Mazzocchi VL, Parente CBR, Valerio MEG, Klimm D. Problems in the thermal investigation of the BaF_2-YF_3 system. *J Therm Anal Calorim.* 2009;95:43–8.
21. Zuzana Netriova, Boca M, Danielik V, Miksikova E. Phase diagram of the system $\text{KF}-\text{K}_2\text{TaF}_7-\text{Ta}_2\text{O}_5$. *J Therm Anal Calorim.* 2009;95:111–5.